TrackMate: An open and extensible platform for single-particle tracking

Jean-Yves Tinevez [a,*], Nick Perry [a,1], Johannes Schindelin [b,2], Genevieve M. Hoopes [c], Gregory D. Reynolds [c], Emmanuel Laplantine [d], Sebastian Y. Bednarek [c], Spencer L. Shorte [a], Kevin W. Eliceiri [b,e]

[a] Imagopole, Citech, Institut Pasteur, 75724 Paris, France
[b] Laboratory for Optical and Computational Instrumentation, University of Wisconsin-Madison, Madison, WI 53706, USA
[c] Department of Biochemistry, University of Wisconsin-Madison, Madison, WI 53706, USA
[d] Laboratory of Signaling and Pathogenesis, Centre National de la Recherche Scientifique, UMR 3691, Institut Pasteur, 75724 Paris, France
[e] Morgridge Institute for Research, Madison, WI 53719, USA

ARTICLE INFO

ABSTRACT

We present TrackMate, an open source Fiji plugin for the automated, semi-automated, and manual tracking of single-particles. It offers a versatile and modular solution that works out of the box for end users, through a simple and intuitive user interface. It is also easily scriptable and adaptable, operating equally well on 1D over time, 2D over time, 3D over time, or other single and multi-channel image variants. TrackMate provides several visualization and analysis tools that aid in assessing the relevance of results. The utility of TrackMate is further enhanced through its ability to be readily customized to meet specific tracking problems. TrackMate is an extensible platform where developers can easily write their own detection, particle linking, visualization or analysis algorithms within the TrackMate environment. This evolving framework provides researchers with the opportunity to quickly develop and optimize new algorithms based on existing TrackMate modules without the need of having to write *de novo* user interfaces, including visualization, analysis and exporting tools.

The current capabilities of TrackMate are presented in the context of three different biological problems. First, we perform *Caenorhabditis-elegans* lineage analysis to assess how light-induced damage during imaging impairs its early development. Our TrackMate-based lineage analysis indicates the lack of a cell-specific light-sensitive mechanism. Second, we investigate the recruitment of NEMO (NF-κB essential modulator) clusters in fibroblasts after stimulation by the cytokine IL-1 and show that photodamage can generate artifacts in the shape of TrackMate characterized movements that confuse motility analysis. Finally, we validate the use of TrackMate for quantitative lifetime analysis of clathrin-mediated endocytosis in plant cells.

1. Introduction

Over the past 30 years, the biological sciences have enjoyed tremendous advances in imaging techniques that provided new insights into dynamic phenomena. Paramount to this significant progress has been the development of novel imaging hardware platforms and fluorescent probes for the visualization of biological processes at the level of whole organisms, single cells, and subcellular. The development of analysis software to extract quantitative data on the dynamics of the processes examined by microscopy has been equally important. In particular, single-particle tracking software – computational tools that can follow objects in a time-lapse movie and quantify their dynamics – are crucial for almost any experiments involving live-cell imaging, and are a critical part of the researcher toolbox.

A number of programs have been designed and have undergone significant refinement over the past several years (some reviewed in [1–3]) for single particle tracking of live cell microscopy images. Furthermore, the importance of tracking in bio-imaging was highlighted by the 2014 IEEE International Symposium on Biomedical Imaging (ISBI) Grand Challenge [4] in which a number of the current approaches for particle tracking were objectively compared.

One important and significant outcome of the ISBI Grand Challenge [4] was that there does not exist at this time a "one-size-fits-all", universally accurate tracking method. Many specific dynamic biological processes require their own specialized tracking tools that can derive and exploit unique aspects of process such as the motion or shape of the tracked objects. This makes the problem of developing a universal tracking method even more challenging; as the accuracy of tracking is inherently dependent on specific parameters, one strategy that works well for a given problem is likely to fail for another one. Therefore, for many live imaging studies, the data analysis will involve generating *de novo* or adapting an existing tracking software method tailored for a single, specific application. However, the efforts required to build tracking software from scratch are considerable. Its development must include: 1) detection tools that can extract objects from images, 2) linking tools that can track these objects over time, 3) visualization tools that can overlay the raw data and tracking results, and 4) analysis tools that can evaluate the results. Additionally, if the goal is to develop a tracking tool that will be widely used within the research community, the software must be user-friendly, developer friendly, modular, validated and interoperable. Given all these hurdles, it is not surprising that only a few tracking algorithms exist [5–13] that are widely available and designed to be useful for the general needs of the greater Life-Science community.

TrackMate is a plugin within the Fiji ImageJ distribution [14] for tracking developed with several concomitant goals. First, it focuses on usability by providing Life-Science researchers with a turnkey user-friendly tracking solution, fulfilling the recommendations of [15]. It is openly available and well documented, and it houses several detection and tracking modules that allow combining manual and automated particle tracking approaches. TrackMate includes several visualization tools as well as other features that facilitate the export and exchange of data and results with other tracking tools and/or analysis applications. Second, TrackMate has been designed for maximal flexibility. The capabilities of TrackMate can be tailored by the user through the addition of specific tracking, detection, visualization, or analysis modules. As a result, researchers can quickly develop a solution suited for their specific application, while taking advantage of existing modules, thus accelerating and facilitating development. Finally, TrackMate uses a data model that makes it a useful tool for a wide range of tracking applications, ranging from single-particle tracking of subcellular organelles to cell lineage analysis. Below we describe the features of TrackMate in more detail and illustrate their application towards three biological use cases that involve tracking and quantification of dynamic live-cell events.

2. Material and methods

2.1. TrackMate: an open and extensible platform for single-particle tracking

2.1.1. Purpose

TrackMate is a Fiji [14] plugin available through this software platform, and therefore benefits from the facilities offered by Fiji for image input/output and preprocessing. TrackMate's main entry point is an interactive plugin where tracking is performed using a wizard-like GUI (Fig. 1). The user is guided through several stages, each of which constitutes a step in the tracking process, choosing what algorithm to use for detection and tracking, and then configuring them. The result of each step is displayed immediately. This allows the user to readily navigate back to readjust settings should the process output be deemed unsatisfactory. Various tools allow for the inspection of intermediate results: a 3D view of the data and the results can be launched, and each particle or track can

be annotated using specific colors to denote numerical values of interest, including *e.g.* particle quality, estimated diameter, track length, track displacement, *etc.* The use of TrackMate is documented in the Supplemental Information of this article.

Manual inspection of tracking results is critical, particularly in practical cases when quantitative metrics are missing, to assess the accuracy of the results. TrackMate contains several visualization tools to ease inspection and facilitate manual curation or editing of the results. The main visualization tool (Fig. 2, top left) overlays the tracking results on the raw image, re-using the ImageJ hyperstack display. A 3D view of the tracking and raw data can also be launched (Fig. 2, bottom left), based on the ImageJ 3D viewer [16]. Finally, TrackScheme was developed to inspect the higher-level structure of tracks (Fig. 2, top and bottom right), which is particularly handy for cell lineages. Much like a train schedule, this tool displays the tracks based only on their links, and lays out spots from bottom to top according to time. Each branching event generates a new vertical lane. Several synchronized views of the same data can be launched and selecting a subset of spots and links will highlight them in all the views.

The main view and TrackScheme also allow direct manual editing of the tracking results. Spots can be moved, added or deleted, and linked or unlinked to tracks. In addition, the spot size can be adjusted, and their names can be changed in batch or individually. Two numerical features keep track of whether a spot or a link has been manually modified.

It is actually possible to entirely skip the detection step or the particle-linking step or both, and generate tracking results *via* manual annotation. A semi-automated tracking tool facilitates manual annotation, by creating the most likely track birthing from a single spot. Any manual modification of the data triggers a recalculation of all the numerical features, so that they are always in sync with the data. Though TrackMate is only a single-particle tracking tool, it ships with basic analysis facilities. Numerical features are calculated for spots, links and tracks automatically and kept up to date when the user manually edits tracks. These numerical features are also used in the GUI for filtering and display and can also be combined in various plots or data tables.

2.1.2. Data model and capabilities

The data model used to store tracking results has constraints strongly affecting what kind of event can be detected at the particle-linking step. A linear data structure such as an array can only represent linear tracks that do not have division or merge events, where two objects fuse into one. Missing detections (also called gaps) however can be handled by storing spot indices in these arrays. In TrackMate the tracking results are represented as a directed simple graph, where vertices are filtered spots generated at the detection step, and edges are links generated at the particle-linking step. This data structure is very flexible and has limited restrictions making it well suited to single-particle tracking. A graph is a structure where vertices (in our case spots) are connected by edges (in our case links across time). In a simple directed graph, a link cannot go from one spot to the same spot and there cannot be more than one link between two spots. Links have a direction going from source spots earlier in time to target spots later in time, and links between two spots in the same frame are forbidden. With such a data structure, a spot can be the source and target to several links, possibly handling cell division events and particle merging events as well.

The generality of this data structure delegates specificity to the subsequent analysis tools. TrackMate can be configured to detect linking, gap-closing, splitting, or merging events and makes no assumption of the biological significance of these events. The subsequent analysis must therefore be tailored to the biological
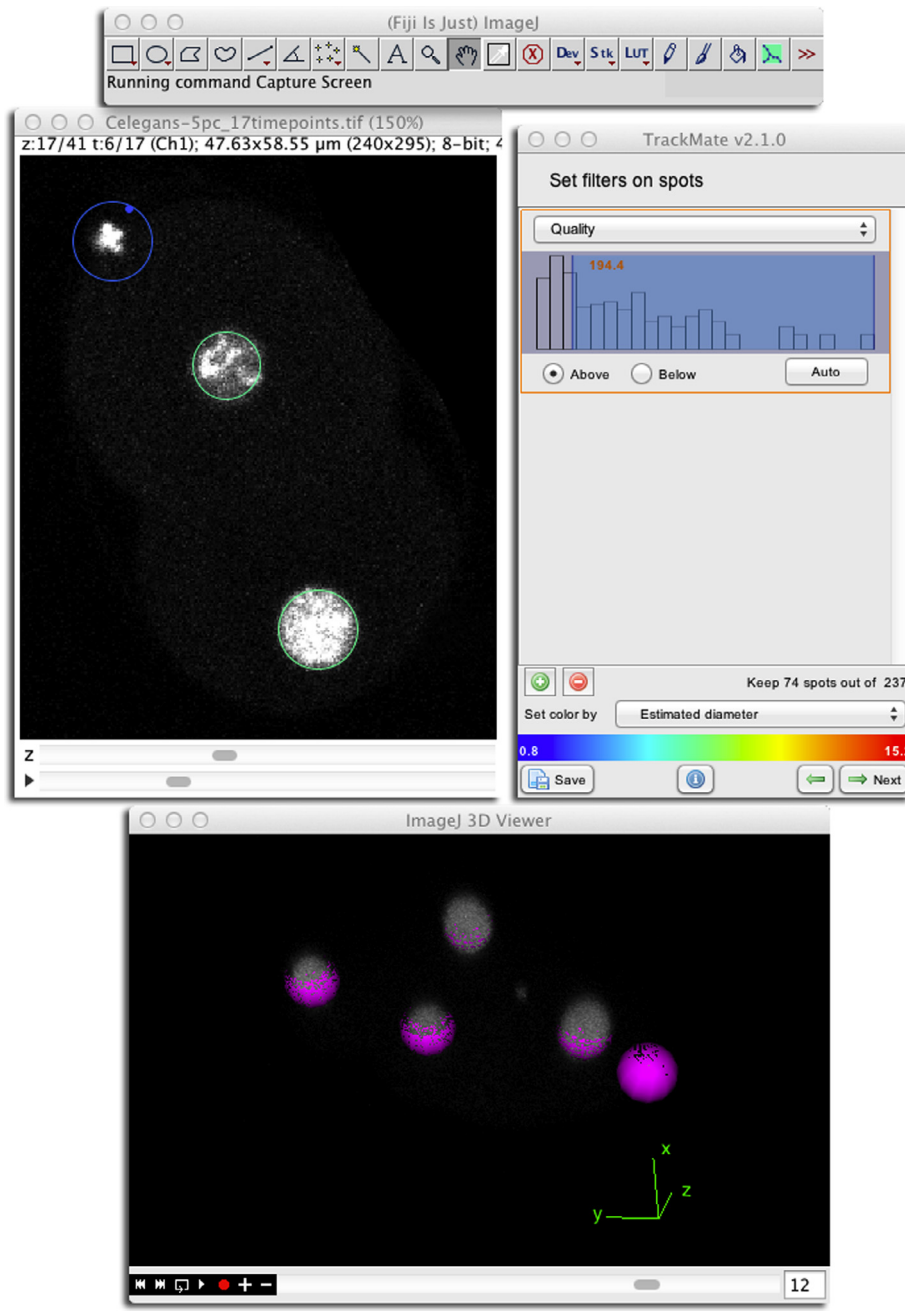
Fig. 1. The TrackMate user interface for automated tracking, depicting the tracking the cells of a developing *C. elegans* embryo. The illustration displays from top to bottom the Fiji toolbar, the image data overlaid with the detection step result and the TrackMate GUI. The central part of the GUI contains the contextual commands for the current tracking step. Here, the user filters out spurious spots based on a quality threshold just after the execution of the detection step. Several filters can be stacked. Detection results, or spots, are represented as spheres with an initially constant radius. Here, the user chose a coloring scheme that reflects an estimate of the true spot radius. The bottom part of the GUI allows the user to navigate forward and backward through the tracking steps, to see a text log of the plugin activity and to save the data at anytime.

problem at hand. TrackMate aims at being as general as possible and encourages end-users to tailor algorithms and analyses specific to their biological problems.

2.1.3. Performance and accuracy

TrackMate ships three classes of particle-linking algorithms. A first class is derived from the LAP framework proposed by Jaqaman and colleagues [7]. Base linking costs are calculated from the square distance between particles, which makes it ideal to tackle Brownian motion [10]. However, costs can be modulated by feature value differences, penalizing the linking of particles that are

different in intensity distribution, rough shape, *etc.* A convenient GUI allows tuning these costs directly in TrackMate. A second particle-algorithm relies on the Kalman filter [17] to tackle linear motion. Finally, particle linking based on nearest-neighbor search is proposed as the simplest linking algorithm.

Accuracy measurements serve as a tool for end-users to choose the optimal algorithm for their specific biological applications. The accuracy of the particle-linking algorithms or spot trackers offered in TrackMate is documented in the Supplemental Information. To establish it, we relied on the ISBI Grand Challenge single-particle tracking dataset [4].
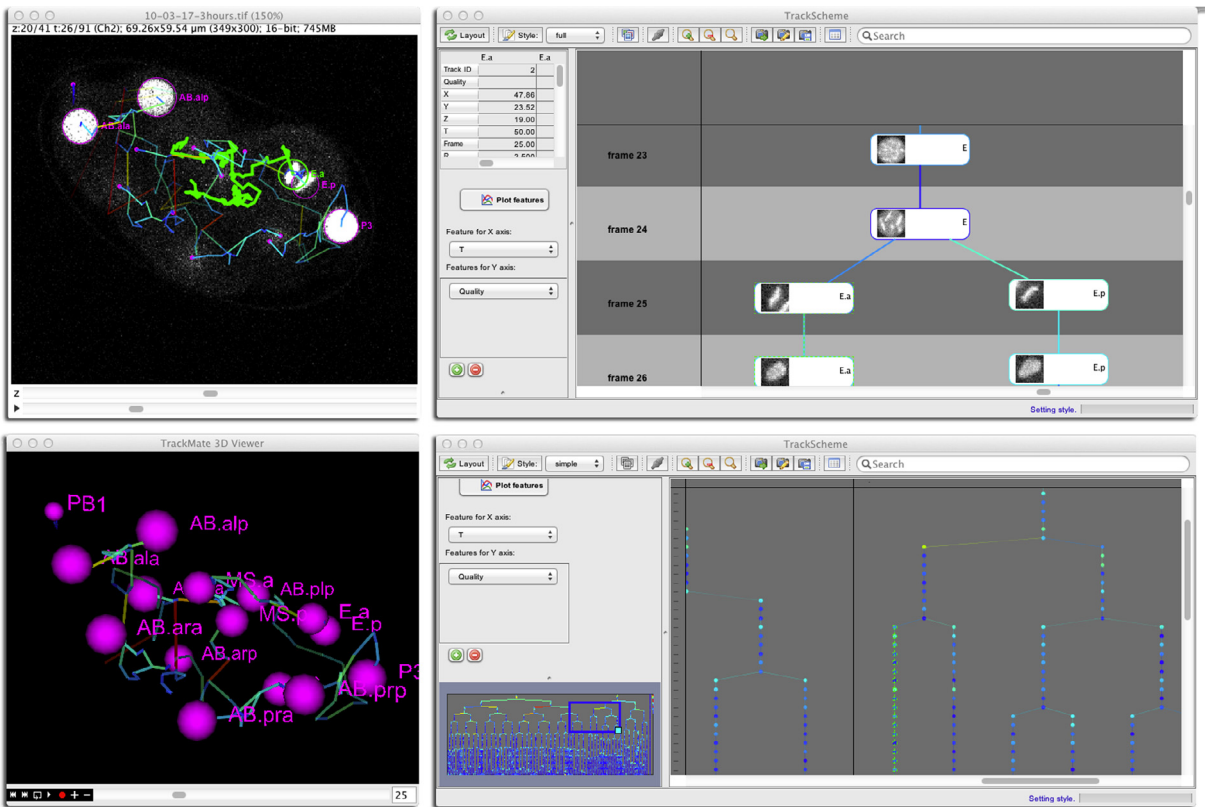
Fig. 2. Four views of the same *C. elegans* embryo being tracked in TrackMate. From left to right then top to bottom: 1. The main TrackMate view, that overlays the tracking results on the raw image window in Fiji. The lineage of the *E.a* founder cell is selected and can be seen as a thick green line. 2. TrackScheme, the track visualization tool of TrackMate. It lays out the tracks in a time oriented hierarchical graph. Here it is centered on the *E* founder cell division and shows the cell names and heir thumbnail. 3. The 3D viewer here shows the TrackMate annotation with cell names. 4. Another instance of TrackScheme, with a higher-level view of the lineage. The edge color encodes the cell displacement in all views from 0 μm (blue) to 5 μm (red). Note that all views are synchronized and share the same selection. (For interpretation of the references to color in this figure legend, the reader is referred to the web version of this article.)

2.1.4. Using TrackMate in scripts and other applications

TrackMate has a modular design that allows using its processing core without relying on the GUI, in scripts or other software. This allows TrackMate to be used for batch analysis, potentially running on a remote cluster over many images at once. The Supplemental Information details the core API of TrackMate and gives examples of scripts in Python and MATLAB. A subset of TrackMate capabilities can also be called using the ImageJ1 macro language.

2.1.5. Interoperability with other software

TrackMate is deployed as a Fiji plugin, and therefore benefits from and interacts with the whole ImageJ ecosystem [18], whether for data import and preprocessing or export and scripting. TrackMate focuses on single-particle tracking, and therefore its end results take the shape of tracks, collections of spots and links. It offers basic track analysis and visualization capabilities, but specific applications are likely to require subsequent, finer analysis, which requires TrackMate files to be interoperable with specialized software. The Fiji distribution of TrackMate ships the files required to import TrackMate results in MATLAB, documented in the Supplemental Information. A specific tool in TrackMate also allows the export of results to a format readable by the Icy software [8]. Alternatively, the Track Manager tool of Icy has an import filter for the TrackMate file format.

2.1.6. Extending and reusing TrackMate

TrackMate is modular in design. Each step in the tracking application corresponds to a module in TrackMate, organized by common interfaces. There are seven types of TrackMate modules, including data visualization, particle detection, particle analysis, particle linking, link analysis, track analysis, and generic actions.

This modular design is made to be extensible. External developers can create their own TrackMate module to fill their own needs. By extending common TrackMate interfaces, they will be integrated in the GUI without distinctions from native modules. TrackMate discovers these new modules automatically thanks to the SciJava annotation framework, which considerably simplifies development. The new modules just need to be annotated with SciJava and compiled as java *jar* files. By dropping the *jar* file in the *plugins* folder of a Fiji installation, they will be automatically discovered by TrackMate and will appear in the GUI. Interestingly, this completely decouples the TrackMate developers from external developers, who can build new modules without requiring intervention. The Supplemental Information documents how to write custom TrackMate modules, covering each of the seven types of module.

2.2. TrackMate and multidimensional imaging

TrackMate was designed for use with multidimensional light microscopy datasets from a wide range of modalities including simple 2D brightfield collection, 3D TIRF imaging, and 4D (space over time) laser scanning microscopy. The program was originally developed for *C. elegans* lineage analysis [19], but has been adapted and widely utilized for a number of other biological tracking applications. Given the wide number of current and possible dynamic imaging uses for TrackMate, in this manuscript we chose to focus

on three applications that showcase the different strengths, features, and potential of TrackMate.

In the first case study, we examine how laser scanning confocal microscopy (LSCM) induced phototoxicity affects cell division in *C. elegans*. By utilizing TrackMate-based cell lineage tracking we can determine whether different imaging doses or techniques can influence the normal cell lineage. This example shows how TrackMate can handle automatic analysis and manual correction. There are many use cases where a fully automatic strategy is not possible due to factors such as variable signal to noise (SNR) in the images. TrackMate was specifically designed to handle 3D data such as this and do automatic – and manual – based cell lineage tracking and analysis.

In the second example we use TrackMate to investigate the ability of NEMO (NF-κB essential modulator), a key component of the NF-κB signaling pathway, to assemble into punctate structures, that we refer as "NEMO dots", upon cell stimulation by cytokines, and how phototoxic effects alter this process even at low illumination doses. NEMO has been shown to be involved in many physiological processes and we have shown that its assembly into punctate structures is an important event of the cell response to pro-inflammatory cytokine stimulation [20]. The formation of NEMO dots is a transient event that occurs rapidly and can be tracked in 2D (using SDCM). A key need for this application is the ability to use the tracking results in subsequent analyses using biophysics methods, revealing the key ability of TrackMate to interoperate with other analysis tools, such as MATLAB.

The third example focuses on clathrin dynamics at the plasma membrane of *Arabidopsis* hypocotyl epidermal cells. In particular, we assess the ability of TrackMate to track the transient recruitment of fluorescent fusion protein tagged clathrin light chain (CLC-FP) into diffraction-limited structures at the plasma membrane and their subsequent release using Variable Angle Epifluorescence Microscopy or TIRFM. This example illustrates on an important trafficking process and the utility of TrackMate in both plant and mammalian models. This use case demonstrates the ability of TrackMate to handle 3D spatial and temporal data, as well as the complex modalities of VAEM/TIRFM time-lapse images. Importantly, in this case study we compare the ability of TrackMate to determine the lifetime of clathrin-coated plasma membrane structures relative to previously-published, manually-tracked CLC-FP foci. Thus, this case study provides a useful validation of TrackMate's tracking accuracy.

2.3. C. elegans embryo imaging

C. elegans embryo imaging was done following the phototoxicity assessment protocol described previously [19]. Briefly: using a LSCM as imaging device (LSM700, Carl Zeiss, Jena, Germany) equipped with a 63x oil NA = 1.4 objective, embryos from the strain AZ212 were imaged at 21 °C. One acquisition made of 41 Z-slices spaced by 1 μm were acquired every 2 min, for at least 2 h starting from the first anaphase. The pixel dwell time was chosen to be 1.58 μs/pixel, and the laser power varied to probe different light doses. The light dose L is calculated as the total energy deposited on the sample for one acquisition; that is:

$$L = P \times dt \times N_{equatorial} \times N_{Zslices}$$

where P is the laser power measured before the objective, assuming nearly perfect transmittance; dt is the pixel dwell time, $N_{equatorial}$ is the number of pixels in the embryo equatorial plane, and $N_{Zslices}$ is the number of Z-slices scanned for a single acquisition.

2.4. NEMO punctate cluster imaging

GFP-NEMO-expressing cells were prepared for live imaging as in [20] and plated in 3.5 cm diameter glass-bottom petri dishes. Two different SDCMs were used for imaging: an UltraVIEW ERS and an UltraVIEW VOX (Perkin-Elmer), based onCSU-22 and CSU-X1 spinning-disks (Yokagawa) respectively, with a EM-CCD camera with a peak QE around 60% (C9100-50, Hamamatsu) and 92% (ImageEM-X2, Hamamatsu), again respectively. A single plane close to the coverslip was chosen for imaging, and the cells were imaged with a PlanApochromat 63x 1.4NA oil objective at 2 frames per second, at 37 °C and 5% CO_2, using a 488 nm laser line and filters suited for the detection of the GFP emission. Stimulation by IL-1 was done at a final concentration of 10 ng/mL.

2.5. VAEM imaging of PM-associated Clathrin dynamics

Sterilized stable transgenic *A. thaliana* ecotype *Wassilewskija* seeds expressing functional Clathrin Light Chain 2-GFP under control of its native promoter [21] were plated on 0.5x Murashige and Skoog Basal Salts 0.5% agar. After vernalization at 4 °C for 72 h, plates were incubated under continuous light at 22 °C for 3 h before being grown in the dark for 5 days. Seedlings were imaged by Variable Angle Epifluorescence Microscopy as described [22] using a Nikon N-STORM Microscope with a motorized TIRF illuminator and Andor iXon Ultra 897 EMCCD camera. Using the TIRFM mode and the 100x oil NA = 1.49 objective, 2D time-lapse sequences were taken at 2 frames per second with 488 nm laser excitation.

3. Results

3.1. C. elegans embryo cell division synchrony and cell cycle length are robust against photodamage

3.1.1. Methods

We recently proposed a quantitative method to assess the phototoxic impact of imaging devices [19]. *C. elegans* embryos have an invariant development pattern, with minimal variation across individuals for the cell lineage, their organization in space, and their division timing [23]. At a temperature of 21 °C and without external perturbation, an embryo develops into a 50-cells organism in two hours measured from the first anaphase. If this process is imaged using a fluorescent strain labeled for nuclei [24], harsh imaging conditions will perturb the normal development and hinder normal progression. For intermediate light doses, this manifests as a delayed development, and less than 50 cells are found after two hours of imaging. We exploited this effect to quantify phototoxic impact: the phototoxic light dose is defined as the energy per acquisition that yield an embryo with 25 cells after 2 h of development at 21 °C. To measure this dose, several embryos were imaged in controlled conditions, changing only the illumination power. The number of cells after 2 h of imaging was plotted against the light dose, and the phototoxic light dose was derived by a fit by a sigmoidal curve [19]. This protocol characterizes the phototoxic impact of an imaging device when imaging 3D specimen over several hours, revealing sensitivities to subtle phototoxic effects. With the laser line used for excitation and the fluorescent labeling of the sample, it reports mainly the fluorescence-sensitized phototoxicity and is not sensitive to any thermal effects that occur for near IR/IR excitation.

While this protocol benchmarks the performance of a system through a bulk measurement on a specimen, determining how photodamage affects specimens requires even deeper insights. We investigate here whether specific cells of the lineage have

different sensitivities to photodamage. This involves building the comprehensive cell lineages, as the embryos sample different light doses. While this task is nowadays greatly facilitated by the pioneering work of other groups [5,25–27], the tools they offer are unfortunately not applicable to our problem. Indeed, the images we generate have a quality that is not adjustable: it is the product of the sensitivity of the system tested and of the light dose probed. For a strong illumination power, the fluorophore quickly bleaches, while this does not happen or not as much for low incident power. A single dataset therefore may have movies with a very low and constant SNR for low light doses, and movies beginning with a strong SNR that quickly decays until the images are no longer exploitable for high light doses (Supplemental Movie 1). To add to this quality discrepancy, a single image of the embryo also shows varying SNR as the Z position of cells vary. Indeed, as we use an oil objective, the image quality quickly deteriorates as the focus moves away from the coverslip. This problem is classically solved by varying the illumination power as the focus moves [25], but again this is not applicable to our study since we want to use a constant illumination power throughout a single experiment.

It is important to note that the extremely high variability in image quality, both in space and time and within a single dataset, is there by construction. As the illumination power is an input variable in our experiments we do not have the liberty to tune it in order to reach a desirable image quality. Rather than develop a highly customized solution that would deal with this issue, we exploited the ability of TrackMate to combine automated and manual annotation approaches. Each movie was first segmented automatically for the cells, and the spurious or missing detections were manually corrected. The curated detection results were then tracked automatically, and tracking mistakes were again manually corrected. The data model of TrackMate directly allows generating lineages, cell divisions being represented by branching events with two links emerging from a mother cell spot. Cells were named following the Sulston and Horvitz convention [28]. Movies with quickly decaying SNR were those for which the automated processing was the less successful, but because they correspond to the toxic light doses, they yielded few cells and the manual correction

took little time. On average, a single acquisition of at least 2 h of development could be lineaged in less than an afternoon. The dataset presented here includes 9 acquisitions, collected on a LSCM, using light doses ranging from 13 µJ/stack to 650 µJ/stack, covering situations where no to extreme phototoxic effects can be observed. A full lineage from this dataset is presented in Supplemental Fig. 2.

3.1.2. Results

The phototoxicity threshold as defined in [19] was found to be 320 µJ/stack for this LSCM, to be compared with the much larger value around 5 mJ/stack that can be measured for epifluorescence-based systems [19,29]. For values well below the phototoxicity threshold, up to 200 µJ/stack, the development of the embryo was virtually non-perturbed (Supplemental Movie 1 and Fig. 3). We investigated how photodamage impacts cell division synchrony and cell cycle length. To do so, we focused on the AB descendants. At 21 °C without imaging, the first two hours of the AB lineage was made of 5 successive divisions that gave rise to 32 descendants. Each of these 5 divisions was well synchronized across sibling cells [23], which allowed for the definition of the cumulative division time for AB_{nx}, the time measured from the first anaphase to the nth division in the AB lineage. This time was characterized by then mean and standard deviation over the n times of division of the n AB_{nx} cells into $2n$ $AB_{(n + 1)x}$ daughter cells.

We first investigated whether or not this synchrony is perturbed by harsh illumination. The cumulative division time is reported in Fig. 3 as a function of the incident light dose. We observed that division synchrony of the AB lineage resists phototoxicity well, as indicated by the very low standard deviation on the division time. Even for disruptive light doses, the AB descendants all divided within 10 min of their siblings. However, close to the phototoxicity threshold and beyond, some cell divisions did not happen at all. This shows that cell division synchrony is robust against photodamage, and more robust than cell division itself.

Surprisingly, cell cycle lengths only vary weakly with light doses. For doses lower than the phototoxicity threshold, the cumulative time to get a specific AB descendant division stayed roughly
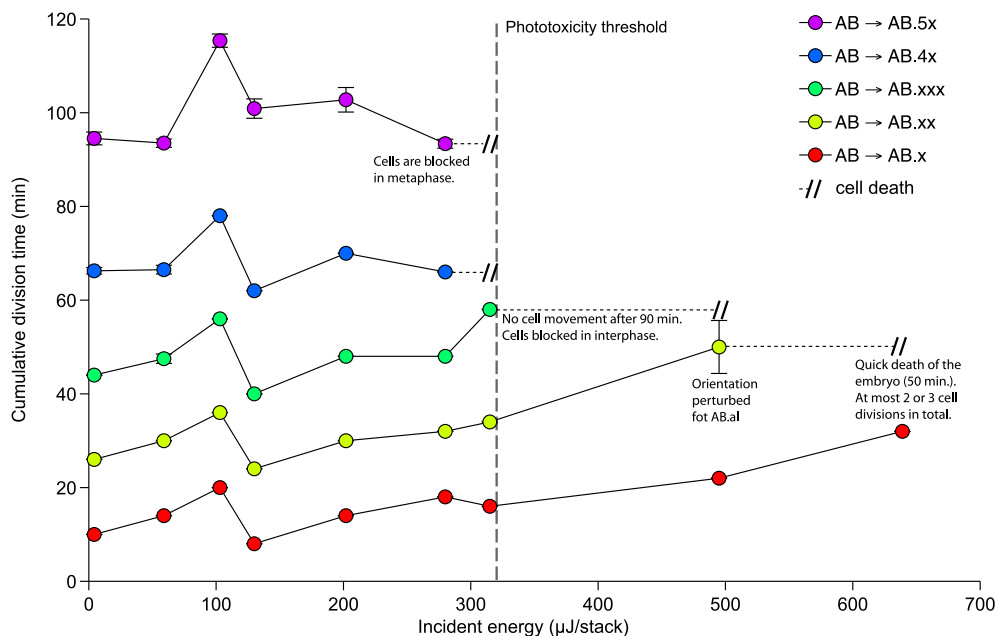

Fig. 3. Cumulative cell division time for the *AB* lineage, measured from the first anaphase in *C. elegans* embryos up to two hours as a function of the incident light dose. Cell division time is defined with mean and standard deviation taken over the times of division of all AB_{nx} cells into $AB_{(n + 1)x}$. A column in this plot represents a single embryo followed over time. Nine embryos were tracked to sample a wide-range of light doses. When a particular cell division does not happen, the assessed reason and notable events are shown as annotations in the plot.

constant (Fig. 3). The observation of [23] in non-invasive conditions still holds, and cell cycle length follows roughly a geometrical sequence, even if it increases slowly with incident light dose. Over the whole range of light doses sampled, the cell cycle time of the AB progenitor doubled. However, this immediate lengthening of division times is not the main feature of phototoxic effects. The embryo development was hindered because for large incident doses, some subsequent cell divisions did not happen. Looking closely at the AB lineage, we saw that for 289 µJ, the $AB_{4x} \rightarrow AB_{5x}$ cell division took place, but the cells were blocked in metaphase. For 324 µJ, the $AB_{3x} \rightarrow AB_{4x}$ did not happen. For 504 µJ, the embryo stopped after $AB_x \rightarrow AB_{xx}$ and for 648 µJ, only the first division of AB happened before the embryo died. Phototoxic effects on a LSCM manifest as a brutal development halt at a certain time depending on the light dose. Before this time is reached, the cycles of cell divisions proceed more-or-less normally.

3.1.3. Discussion

The robustness of the synchrony and of the order of cell divisions indicates that there probably is not a cell-dependent sensitivity to phototoxic effects, at least for the AB descendants. Photodamage affects all cells in a similar manner. Embryonic cell proliferation involves rapid cell divisions through short cell cycles, most of which lack G1 and G2 phases [30]. By construction, our phototoxicity assay targets damage to the nucleus and is likely to cause first DNA damage. But the embryonic cell division of misses robust checkpoints for DNA damage [30], which explains why the lengths of cell cycles only depend weakly on incident light doses. The catastrophic arrest of cell divisions might reflect harsher damage affecting the structural components of the mitosis. Therefore, even if we introduced as a sensitive specimen for our phototoxicity assay, our photodamage readout probably misses subtle DNA damage happening at low doses.

3.2. NEMO-IKK structures dynamics is adversely affected by subtle phototoxic damage

NEMO (NF-κB Essential Modulator) is a critical component of the NF-κB signaling pathway and is a key actor of many physiological processes such as immune response, inflammation, cell survival and proliferation [31]. We recently observed that upon stimulation by various cytokines, NEMO rapidly and transiently assembles into punctate structures [20]. Thanks to cell lines that stably express GFP-NEMO, this process can be investigated via imaging and single-particle tracking, opening the way to analyzing these structures via biophysical methods complementary to biochemical approaches. Using imaging we quantified the dynamics of the NEMO dots, showing that they experience a rapid turnover of their molecular content, and that they are anchored in the vicinity of the cell membrane [20]. These results are critical to our understanding of the process leading to the activation of the NEMO-IKK complex, as a part of the NF-κB pathway.

A downside of fluorescence microscopy as described in our first case study is that it can be invasive, altering the physiology of the organism and/or cells due to phototoxicity, thereby affecting the process understudy. In particular it can affect the motion dynamics of organelles, potentially including the NEMO dots. We investigate here how phototoxicity impacts these dynamics and leads to an erroneous conclusion on the motion model of the NEMO subcellular structures.

3.2.1. Results

Two SDCMs were used to image human cells constitutively expressing GFP-NEMO, each with a different light dose range (low intensities: 14–40 µJ, high intensities: 500–700 µJ). Upon the addition of the IL-1 cytokine (10 ng/ml final), the NEMO

superstructures appear as bright, punctate, diffraction-limited dots over a fainter background. These dots were tracked using TrackMate until they disappeared. Subsequently, the tracks were imported and analyzed in MATLAB. Their time-course is displayed on Fig. 4a. In the case of high intensities, fewer dots were observed per cell, but they remained for a much longer time. For low intensities, they appeared and disappeared in less than 15 min measured from the addition of IL-1, whereas for high intensities, they lasted for more than 30 min.

Their motion characteristics also differed under high versus low intensity illumination. In both cases, they display random rapid movements, but over longer time scales in the case of high intensities, many of them display large, directed movements, sometimes over 10 µm, preferably oriented towards the nucleus (Supplemental Movie 2). At low intensities, they all remained within 2 µm of their average position for their whole lifetime (Supplemental Movie 3). The movement of the NEMO dots was quantified and
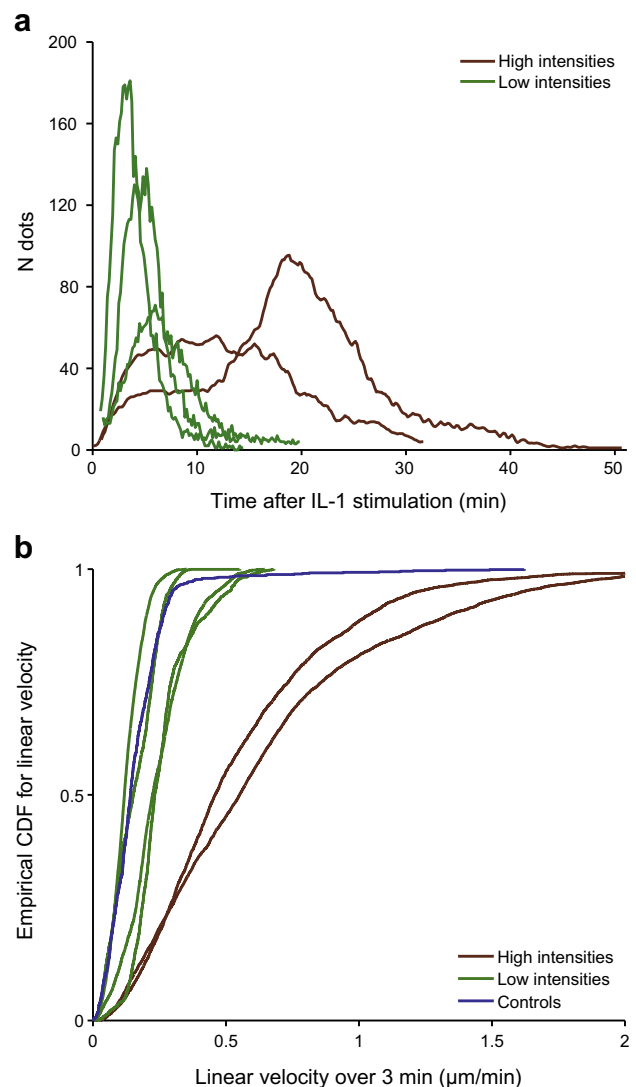
Fig. 4. a. NEMO dots dynamics over time, measured from the addition of IL-1 (10 ng/mL final), comparing high and low illumination intensities. Each line counts the number of NEMO dots in a single cell. b. Empirical cumulative distribution (CDF) of the linear velocity of NEMO dots for several cells after stimulation by IL-1. Linear velocity is defined for each NEMO dot as the median of all its 3 min-displacements divided by a 3 min interval. Each line is the CDF for all the NEMO dots of a single cell. The blue line, termed 'Controls', plots the CDF of the linear velocity of unspecific dots undergoing Brownian motion in a non-stimulated cell.

expressed in terms of linear velocity, a measure of how far a particle moves over a period of time. Here the linear velocity of a NEMO dot was defined as the median of all the 3 min-displacement of this dot, divided by an interval of 3 min.

The empirical cumulative distribution function for all cells is displayed in Fig. 4b. For low intensities, the linear velocity is in the range of 0.11–0.23 µm/min (4 cells, 939 NEMO dots). This value is in the range of the linear velocity measured on dots of a control, non-stimulated cell, 0.14 µm/min (1 cell, 17 dots). These dots are non-functional NEMO aggregates typically found in cells highly expressing GFP-NEMO, and undergo Brownian random motion. For high intensities the linear velocity ranges from 0.45 to 0.56 µm/min (2 cells, 325 NEMO dots), with some values as large as 2 µm/min. The fact that under high illumination NEMO dots can have large directed movements suggests that they are actively transported in these conditions.

To confirm this observation, we performed mean-square-displacement (MSD) analysis comparing NEMO dots under high and low illumination intensities. The fit of the log-log plot the MSD curves yielded a factor α that determines whether the dots are bound to a fixed structure ($\alpha < 1$), freely diffused ($\alpha \approx 1$) or actively transported ($\alpha > 1$) [32]. We retained dots for which the R^2 value of the log-log fit is larger than 0.8. The values of all dots were pooled together for a cell, and we assessed the motion type for this cell using a t-test. We found that for high intensities, all cells have a α value significantly larger than 1 ($p = 10^{-3}$–10^{-4}), indicating that NEMO dots are actively transported. However, the α value for cells illuminated with low intensities have a α value significantly lower than 1 ($p < 10^{-10}$).

3.2.2. Discussion

The range of low versus high illumination intensities in this study is dictated by the sensitivity of the cameras equipping the two different microscope systems utilized. One was equipped with a very sensitive camera with high quantum efficiency, allowing for using low intensities to track NEMO superstructures. The other camera had a more modest quantum efficiency, and prompted for larger illumination intensities. However, even the high intensities used on the second system are not extremely high in absolute value. The phototoxic light dose measured on this system is about 21 mJ [19]. The equivalent light dose used in this study extrapolated over 2 min was in the range 60–80 mJ. We therefore used an illumination dose larger than the phototoxic threshold according to [19], but well within an order of magnitude. For low intensities, the equivalent light dose over 2 min is in the range 8.4–24 mJ. This difference was enough to separate results in two completely different categories, one of which is evidently corrupted by artifacts.

The NEMO dots display longer dynamics in cells exposed to high light intensities, which we attribute to artifactual cell stimulation by light-induced stress. The large displacements observed at high intensities are likely to be due to cell shrinking in response to phototoxicity. The dots may follow the cell membrane as the cell shrinks and display an artifactual motion, which resembles a directed movement towards the nucleus. An erroneous interpretation of these artifacts is that following stimulation by IL-1, NEMO is assembled into membrane-associated superstructures that are subsequently actively transported towards the nucleus. However, biochemical studies showed that the NEMO structures are most likely anchored to the cell membrane for their entire lifetimes, which is confirmed by MSD analysis when under non-invasive imaging condition [20]. Phototoxicity effects can give artifactual results that yield erroneous conclusions and strongly compromise interpretation of the role of a molecule.

3.3. VAEM imaging of plasma membrane-associated Clathrin dynamics in Arabidopsis

Secretory and endocytic membrane trafficking are essential processes critical for growth and development of multicellular organisms including cell expansion and division, as well as responses to abiotic and biotic signals. Bidirectional trafficking of cargo materials between the discrete organelles of the secretory and endocytic pathways is primarily mediated by vesicular carriers. Clathrin, a vesicle coat protein complex, is responsible for cargo selection and formation of vesicles that traffic between the plasma membrane, endosome, trans-Golgi, and the vacuole [33,34]. Clathrin-coated vesicle (CCV) formation involves the temporal and highly ordered assembly of proteins following a poorly understood nucleation event. After this site-selecting initiation event, cargo begins to cluster together on the membrane through the action of various cargo receptors and adaptor complexes specific to each trafficking pathway (i.e. the adaptin 2, AP2, and TPLATE complexes in clathrin mediated endocytosis, CME, in plants [35]). While well characterized in yeast and mammalian systems, less is known of the molecular underpinnings of clathrin-dependent vesicle formation and targeting in plants.

Clathrin-mediated endocytosis (CME), cytoskeletal dynamics, and other events occurring at the cell cortex have been successfully imaged in mammalian and other systems using Total Internal Reflection Fluorescence Microscopy (TIRFM [36]). Likewise, TIRFM has been utilized to image molecular events at or adjacent to the cell cortex in plant cells [37]. However, plant cells are non-ideal samples for TIRFM analysis owing to the thickness of plant cell walls, which can exceed 500 nm, the theoretical limit of TIRFM illumination, and the non-uniform refractive index of cell walls due to variations in composition between cell types and stages of development. Additionally, plants do not readily adhere to glass surfaces, which, in combination with frequently non-uniform geometries of plant tissues, make the task of imaging molecular events at the cell cortex in single plant cells by the critical angle illumination necessary for TIRFM challenging. To accommodate these technical hurdles, Variable Angle Epifluorescence Microscopy (VAEM), which utilizes sub-critical laser angles to achieve oblique illumination of the plant cell cortex, was developed as an alternative application of TIRFM systems [22]. Essentially, the incident angle of the excitation beam utilized for VAEM is adjusted to generate an uneven 'wedge' of illumination radiating from the optical axis. The result is the maintenance of high S/N ratio at greater illumination depths (>1000 nm) than are achievable with TIRFM [22].

3.3.1. Results

Here, we employ TrackMate to analyze VAEM data of fluorescently tagged clathrin foci at the cell cortex to compare the software's particle tracking capabilities of manually chosen plasma membrane PM-associated clathrin foci with completely manually processed data. Representative images demonstrate CLC2-GFP foci labeling of PM foci and larger cortical Golgi structures (Fig. 5a and b) in Arabidopsis hypocotyl epidermal cells. The clathrin containing PM foci have a more uniform fluorescence and are diffraction limited in size compared to the larger CLC2-GFP labeled Golgi structures, displaying the characteristic fluorescence profile of sites of CME previously described [21]. Three independent hypocotyls were imaged and time-lapse images from each were analyzed manually and semi-automatically with TrackMate (Supplemental Movie 4). A histogram comparing the manual and TrackMate data displays the distribution of clathrin PM foci lifetimes observed by both methods (Fig. 5c). PM-associated clathrin foci lifetimes determined manually and via TrackMate range from 5–50 s and 7–55 s, respectively. The medians of the manual and TrackMate generated lifetimes are 20.5 s and 22.3 s, respectively.
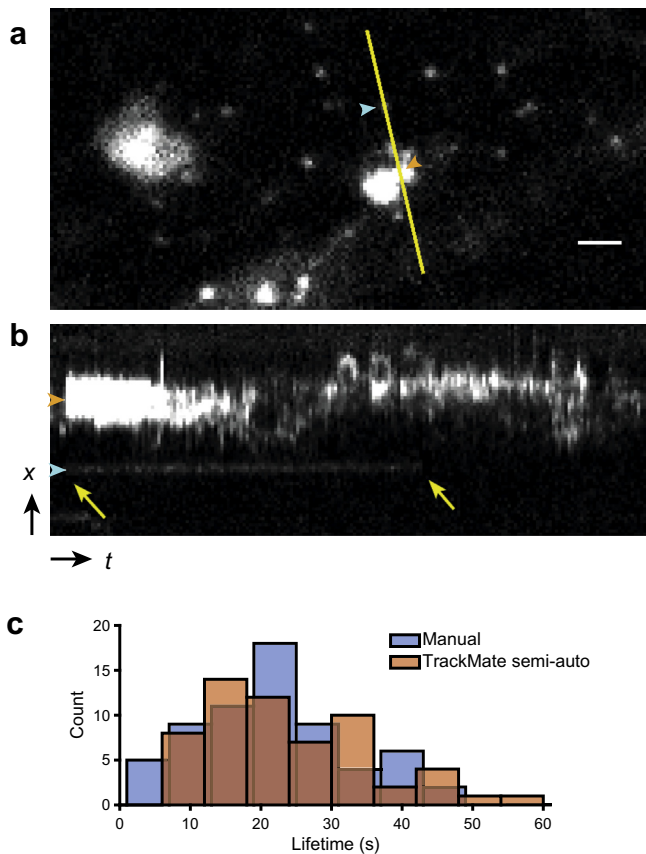
deviation, N = 64) and 24.2 ± 11.6 s (N = 59), respectively. The Student's *t*-test and the Kolmogorov–Smirnov test gave both gave p-values greater than 0.1.

3.3.2. Discussion

Previously, the lifetimes of CLC2-GFP positive PM foci were determined by manual identification and quantitation of the fluorescence intensity of individual foci across a time-lapse series of images; a laborious and potentially biased process plagued by the difficult and somewhat arbitrary determination of where events begin and end. TrackMate helps in addressing these issues through its ability to follow a single focus throughout its whole lifetime from a single manual annotation. The slight difference between the manual and TrackMate average clathrin foci lifetimes is most likely due to TrackMate's capability to detect foci beyond what the human eye can discern via the quality threshold parameter. Despite this slight difference, the Student's *t*-test and the Kolmogorov–Smirnov test indicate that the manual and TrackMate average lifetime values and data distribution do not statistically differ from each other for PM associated Clathrin foci. This suggests that the software's tracking capabilities are compatible with manual tracking of clathrin dynamics at the PM. A number of laboratories studying clathrin and clathrin accessory proteins involved in plant CME have found the average lifetime of clathrin-associated PM foci to range from 17.7 s to 24 s, corroborating the average lifetime of clathrin foci at the PM found both manually and semi-automatically with TrackMate [21,38,39]. Inevitably, TrackMate's ability to objectively track foci is dependent upon parameters defined by the operator thereby introducing some level of bias into the results. Nevertheless, these parameters can be universally applied across all samples, eliminating unintentional precision errors and eye-constrained selection of track termination. Taken together, this data demonstrates the utility of TrackMate in alleviating a previously laborious analysis of dynamic events in microscopy data.

Fig. 5. VAEM imaging of clathrin foci in *Arabidopsis* hypocotyl epidermal cells. a. Single image of a time-lapse movie following the lifetime of clathrin foci. The fluorescence signal shows clathrin foci along with larger, brighter Golgi structures. Yellow line: profile used for the kymograph in b. Scale bar: 2 μm. Blue and orange arrowheads denote PM- and Golgi-associated clathrin, respectively. b. Kymograph extracted along the yellow line in a. The brightness has been adjusted to better show the clathrin focus, saturating the display of the large Golgi structure. Yellow arrows: start and end of the clathrin focus lifetime, determined manually. Blue and orange arrowheads denote PM- and Golgi-associated clathrin, respectively. c. Histograms of lifetimes for clathrin foci.

The average foci lifetimes for each individual hypocotyl did not vary significantly and the average foci lifetimes for manual and TrackMate data over all samples are 21.7 ± 10.5 s (mean ± standard

4. Discussion

TrackMate has been used in protein motility studies [40,41], molecular motor tracking [42], axonal transport [43], sperm cell tracking [44], Golgi bodies tracking [45] in plants, wound healing [46], bacterial biofilm micro-rheology [47], cell movement on stiffness-patterned substrate [48], cell tracking in zebrafish [49] and drosophila [50] embryos, infected cells tracking [51], colloid

Table 1
User contributed modules of TrackMate v3.4.0.

Module name	Module type	Purpose	Author	Location
Linear tracker	Particle-linking	Linking transported particles by extrapolating their velocity	Ronny Sczech	https://github.com/chicoronny/RonnyTrackMate
Batch mode	Plugin	Runs TrackMate in batch, reading configuration from a file		
Binary detector	Spot detector	Detect spot using intensity thresholding and ImageJ particle analyzer		
CSV exporter	Generic action	Export tracks to CSV file		
SQLite exporter	Generic action	Export tracks to SQLite database		
Multi-channel intensity analyzer	Spot feature analyzer	Compute spot mean intensity in up to 10 channels	Benoit Lombardot	https://github.com/tinevez/TrackMate-extras
Find maxima	Spot detector	Detection based on region growing, reimplementing ImageJ *Find maxima* command	Thorsten Wagner	http://imagej.net/Find_maxima_(TrackMate_module)
Trajectory classifier	Plugin	Classify 2D tracks into normal diffusion, subdiffusion, confined diffusion and directed/active motion by a random forest approach		https://github.com/thorstenwagner/ij-trajectory-classifier
Close gaps	Generic action	Close gaps in tracks by creating spots in missing frame by linear interpolation of their coordinates	Robert Haase	Integrated into TrackMate v3.4.0

diffusion studies [52], carboxysome lineaging in cyanobacteria [53], magnetic bead aggregates tracking in arteries [54], diatom motility studies [55], and stretch measurements in biomedical materials [56]. It also enabled the biological studies presented here, investigating the presence of a cell-specific phototoxic effect on embryonic development, the impact of phototoxicity on the dynamics of NEMO dot assembly and the dynamics of clathrin-mediated endocytic events in plant cells.

This great breadth of applications highlights the vast applicability of TrackMate. Generality often has a toll on the ability to successfully handle very specific problems. As noted in [4], it is very likely that some tracking challenges will require the development of specific tracking tools. TrackMate positions itself not only as a tool for single-particle tracking, but also as a platform to facilitate and accelerate the development of such tools. Other developers can port their algorithm(s) to TrackMate as a module, reusing the facilities there that would otherwise consume countless and tedious time to develop (data model, visualization, *etc.*). The SciJava annotation mechanism used for plugin discovery ensures that new modules can be developed and distributed without requiring any interaction with the TrackMate developers, ensuring full autonomy and independence. As of today, we are aware of four groups of contributions made public, listed in Table 1.

5. Future directions

TrackMate was first developed as a lineage tool in *C. elegans* and largely extended to deal with other problems such as intra- and inter-cellular trafficking. As discussed above TrackMate is being widely used, but to remain most relevant, its development needs to continue, in order to deal with emerging data types, scales, modalities, and analysis workflows. Many of these problems can be readily solved by how TrackMate is developed and deployed. By being an open source Fiji plugin that uses modular libraries such as Bio-formats [57], SciJava [18], ImgLib2 [58], *etc.*, it is relatively straightforward to adapt TrackMate to new modalities and use cases. However, there are some challenges that may necessitate augmenting TrackMate's capabilities. For example, it is interesting to not only look at varying temporal scales but also at varying spatial scales. As multiscale imaging methods are developed and deployed to look at process such as metastasis and cell growth, there will need to be corresponding modules that can track and analyze these processes over different spatial scales.

As well, TrackMate needs to continue to evolve in its interoperability and ability to handle heterogeneous data, including non-image data types. One strategy that has served TrackMate well that we will continue to leverage is to take advantage of existing software tools and also offer TrackMate as a flexible portable module. In future development, we hope to have TrackMate equally accessible not only as a Fiji plugin but as an Ops module [18]. The ImageJ Ops initiative aims at producing a unifying library for scientific image processing, and makes it widely accessible to any software framework, not just ImageJ. The Ops framework provides unified interfaces for basic image manipulations that can be called by any tool using this framework. This type of modularity has already shown considerable promise in the recent use of TrackMate in KNIME as a SciJava process [59]. By having TrackMate in KNIME, it is possible to create data pipelines that could integrate Track-Mate with a number of other tools including statistical tools such as R. With the recently developed Ops framework being driven by the ImageJ2 and KNIME developer community, it should be possible to take TrackMate functionality even farther and to a wider audience. In this way, other programs such as databases and even other tracking programs could call TrackMate, much in the same way that programs invoke scripts and other algorithms.

Recent developments in light microscopy, such as light sheet microscopy [60], have resulted in massive datasets that in requires large extensive annotations. These requirements will demand a new type of data model that can support this type of extension annotation in 2D and 3D. Our hope is that such a data model could be driven and utilized by a number of common tools, including TrackMate.

Appendix A. Supplementary data

Supplementary data associated with this article can be found, in the online version, at http://dx.doi.org/10.1016/j.ymeth.2016.09.016.

References

[1] E. Meijering, I. Smal, G. Danuser, Tracking in molecular bioimaging, IEEE Signal Proc. Mag. 23 (3) (2006) 46–53.
[2] N. Chenouard, A. Dufour, J.C. Olivo-Marin, Tracking algorithms chase down pathogens, Biotechnol. J. 4 (6) (2009) 838–845.
[3] Y. Kalaidzidis, Intracellular objects tracking, Eur. J. Cell Biol. 86 (9) (2007) 569–578.
[4] N. Chenouard, I. Smal, F. de Chaumont, M. Maska, I.F. Sbalzarini, Y. Gong, J. Cardinale, C. Carthel, S. Coraluppi, M. Winter, A.R. Cohen, W.J. Godinez, K. Rohr, Y. Kalaidzidis, L. Liang, J. Duncan, H. Shen, Y. Xu, K.E. Magnusson, J. Jalden, H.M. Blau, P. Paul-Gilloteaux, P. Roudot, C. Kervrann, F. Waharte, J.Y. Tinevez, S.L. Shorte, J. Willemse, K. Celler, G.P. van Wezel, H.W. Dan, Y.S. Tsai, C. Ortiz de Solorzano, J.C. Olivo-Marin, E. Meijering, Objective comparison of particle tracking methods, Nat. Methods 11 (3) (2014) 281–289.
[5] J.I. Murray, Z. Bao, T.J. Boyle, R.H. Waterston, The lineaging of fluorescently-labeled Caenorhabditis elegans embryos with StarryNite and AceTree, Nat. Protoc. 1 (3) (2006) 1468–1476.
[6] D. Sage, F.R. Neumann, F. Hediger, S.M. Gasser, M. Unser, Automatic tracking of individual fluorescence particles: application to the study of chromosome dynamics, IEEE Trans. Image Process. 14 (9) (2005) 1372–1383.
[7] K. Jaqaman, D. Loerke, M. Mettlen, H. Kuwata, S. Grinstein, S.L. Schmid, G. Danuser, Robust single-particle tracking in live-cell time-lapse sequences, Nat. Methods 5 (8) (2008) 695–702.
[8] F. de Chaumont, S. Dallongeville, N. Chenouard, N. Herve, S. Pop, T. Provoost, V. Meas-Yedid, P. Pankajakshan, T. Lecomte, Y. Le Montagner, T. Lagache, A. Dufour, J.C. Olivo-Marin, Icy: an open bioimage informatics platform for extended reproducible research, Nat. Methods 9 (7) (2012) 690–696.
[9] N. Chenouard, I. Bloch, J.C. Olivo-Marin, Multiple hypothesis tracking for cluttered biological image sequences, IEEE Trans. Pattern Anal. 35 (11) (2013) 2736–2750.
[10] J.C. Crocker, D.G. Grier, Methods of digital video microscopy for colloidal studies, J. Colloid Interface Sci. 179 (1) (1996) 298–310.
[11] A. Serge, N. Bertaux, H. Rigneault, D. Marguet, Dynamic multiple-target tracing to probe spatiotemporal cartography of cell membranes, Nat. Methods 5 (8) (2008) 687–694.
[12] I.F. Sbalzarini, P. Koumoutsakos, Feature point tracking and trajectory analysis for video imaging in cell biology, J. Struct. Biol. 151 (2) (2005) 182–195.
[13] F.P. Cordelières, V. Petit, M. Kumasaka, O. Debeir, V. Letort, S.J. Gallagher, L. Larue, Automated cell tracking and analysis in phase-contrast videos (iTrack4U): development of Java software based on combined mean-shift processes, PLoS ONE 8 (11) (2013) e81266.
[14] J. Schindelin, I. Arganda-Carreras, E. Frise, V. Kaynig, M. Longair, T. Pietzsch, S. Preibisch, C. Rueden, S. Saalfeld, B. Schmid, J.Y. Tinevez, D.J. White, V. Hartenstein, K. Eliceiri, P. Tomancak, A. Cardona, Fiji: an open-source platform for biological-image analysis, Nat. Methods 9 (7) (2012) 676–682.

[15] A.E. Carpenter, L. Kamentsky, K.W. Eliceiri, A call for bioimaging software usability, Nat. Methods 9 (7) (2012) 666–670.

[16] B. Schmid, J. Schindelin, A. Cardona, M. Longair, M. Heisenberg, A high-level 3D visualization API for Java and ImageJ, BMC Bioinformatics 11 (2010) 274.

[17] R.E. Kalman, A new approach to linear filtering and prediction problems, J. Basic Eng. 82 (1) (1960) 35–45.

[18] J. Schindelin, C.T. Rueden, M.C. Hiner, K.W. Eliceiri, The ImageJ ecosystem: An open platform for biomedical image analysis, Mol. Reprod. Dev. 82 (7–8) (2015) 518–529.

[19] J.Y. Tinevez, J. Dragavon, L. Baba-Aissa, P. Roux, E. Perret, A. Canivet, V. Galy, S. Shorte, A quantitative method for measuring phototoxicity of a live cell imaging microscope, Methods Enzymol. 506 (2012) 291–309.

[20] N. Tarantino, J.Y. Tinevez, E.F. Crowell, B. Boisson, R. Henriques, M. Mhlanga, F. Agou, A. Israel, E. Laplantine, TNF and IL-1 exhibit distinct ubiquitin requirements for inducing NEMO-IKK supramolecular structures, J. Cell Biol. 204 (2) (2014) 231–245.

[21] C.A. Konopka, S.K. Backues, S.Y. Bednarek, Dynamics of arabidopsis dynamin-related protein 1C and a clathrin light chain at the plasma membrane, Plant Cell 20 (5) (2008) 1363–1380.

[22] C.A. Konopka, S.Y. Bednarek, Variable-angle epifluorescence microscopy: a new way to look at protein dynamics in the plant cell cortex, Plant J. 53 (1) (2008) 186–196.

[23] Z. Bao, Z. Zhao, T.J. Boyle, J.I. Murray, R.H. Waterston, Control of cell cycle timing during C. elegans embryogenesis, Dev. Biol. 318 (1) (2008) 65–72.

[24] V. Praitis, E. Casey, D. Collar, J. Austin, Creation of low-copy integrated transgenic lines in Caenorhabditis elegans, Genetics 157 (3) (2001) 1217–1226.

[25] Z. Bao, J.I. Murray, T. Boyle, S.L. Ooi, M.J. Sandel, R.H. Waterston, Automated cell lineage tracing in Caenorhabditis elegans, Proc. Natl. Acad. Sci. U.S.A. 103 (8) (2006) 2707–2712.

[26] S.G. Megason, In toto imaging of embryogenesis with confocal time-lapse microscopy, Methods Mol. Biol. 546 (2009) 317–332.

[27] R. Schnabel, H. Hutter, D. Moerman, H. Schnabel, Assessing normal embryogenesis in Caenorhabditis elegans using a 4D microscope: variability of development and regional specification, Dev. Biol. 184 (2) (1997) 234–265.

[28] J.E. Sulston, H.R. Horvitz, Post-embryonic cell lineages of the nematode, Caenorhabditis elegans, Dev. Biol. 56 (1) (1977) 110–156.

[29] J. Caron, C. Fallet, J.Y. Tinevez, L. Moisan, L.P. Braitbart, G.Y. Sirat, S.L. Shorte, Conical diffraction illumination opens the way for low phototoxicity super-resolution imaging, Cell Adhes. Migr. 8 (5) (2014) 430–439.

[30] E.T. Kipreos, C. elegans cell cycles: invariance and stem cell divisions, Nat. Rev. Mol. Cell Biol. 6 (10) (2005) 766–776.

[31] M.S. Hayden, S. Ghosh, NF-κB, the first quarter-century: remarkable progress and outstanding questions, Genes Dev. 26 (3) (2012) 203–234.

[32] H. Qian, M.P. Sheetz, E.L. Elson, Single particle tracking. Analysis of diffusion and flow in two-dimensional systems, Biophys. J. 60 (4) (1991) 910–921.

[33] X. Chen, N.G. Irani, J. Friml, Clathrin-mediated endocytosis: the gateway into plant cells, Curr. Opin. Plant Biol. 14 (6) (2011) 674–682.

[34] G.A. Baisa, J.R. Mayers, S.Y. Bednarek, Budding and braking news about clathrin-mediated endocytosis, Curr. Opin. Plant Biol. 16 (6) (2013) 718–725.

[35] Y. Zhang, S. Persson, J. Hirst, M.S. Robinson, D. van Damme, C. Sanchez-Rodriguez, Change your TPLATE, change your fate: plant CME and beyond, Trends Plant Sci. 20 (1) (2015) 41–48.

[36] T. Kirchhausen, Imaging endocytic clathrin structures in living cells, Trends Cell Biol. 19 (11) (2009) 596–605.

[37] G. Vizcay-Barrena, S.E.D. Webb, M.L. Martin-Fernandez, Z.A. Wilson, Subcellular and single-molecule imaging of plant fluorescent proteins using total internal reflection fluorescence microscopy (TIRFM), J. Exp. Bot. 62 (15) (2011) 5419–5428.

[38] L. Bashline, S. Li, C.T. Anderson, L. Lei, Y. Gu, The endocytosis of cellulose synthase in arabidopsis is dependent on μ2, a clathrin-mediated endocytosis adaptin, Plant Physiol. 163 (1) (2013) 150–160.

[39] A. Gadeyne, C. Sánchez-Rodríguez, S. Vanneste, S. Di Rubbo, H. Zauber, K. Vanneste, J. Van Leene, N. De Winne, D. Eeckhout, G. Persiau, E. Van De Slijke, B. Cannoot, L. Vercruysse, Jonathan R. Mayers, M. Adamowski, U. Kania, M. Ehrlich, A. Schweighofer, T. Ketelaar, S. Maere, Sebastian Y. Bednarek, J. Friml, K. Gevaert, E. Witters, E. Russinova, S. Persson, G. De Jaeger, D. Van Damme, The TPLATE adaptor complex drives clathrin-mediated endocytosis in plants, Cell 156 (4) (2014) 691–704.

[40] M.E. Tanenbaum, L.A. Gilbert, L.S. Qi, J.S. Weissman, R.D. Vale, A protein-tagging system for signal amplification in gene expression and fluorescence imaging, Cell 159 (3) (2014) 635–646.

[41] M.F. Mossuto, S. Sannino, D. Mazza, C. Fagioli, M. Vitale, E.D. Yoboue, R. Sitia, T. Anelli, A dynamic study of protein secretion and aggregation in the secretory pathway, PLoS ONE 9 (10) (2014) e108496.

[42] A. Reversat, M.I. Yuseff, D. Lankar, O. Malbec, D. Obino, M. Maurin, N.V. Penmatcha, A. Amoroso, L. Sengmanivong, G.G. Gundersen, I. Mellman, F. Darchen, C. Desnos, P. Pierobon, A.M. Lennon-Duménil, Polarity protein Par3 controls B-cell receptor dynamics and antigen extraction at the immune synapse, Mol. Biol. Cell 26 (7) (2015) 1273–1285.

[43] S. Gluska, M. Chein, N. Rotem, A. Ionescu, E. Perlson, Tracking Quantum-Dot labeled neurotropic factors transport along primary neuronal axons in compartmental microfluidic chambers, Methods Cell Biol. 131 (2016) 365–387.

[44] P. Denninger, A. Bleckmann, A. Lausser, F. Vogler, T. Ott, D.W. Ehrhardt, W.B. Frommer, S. Sprunck, T. Dresselhaus, G. Grossmann, Male-female communication triggers calcium signatures during fertilization in Arabidopsis, Nat. Commun. 5 (2014) 4645.

[45] B. Sporsheim, A. Øverby, A.M. Bones, Allyl isothiocyanate inhibits actin-dependent intracellular transport in Arabidopsis thaliana, Int. J. Mol. Sci. 16 (12) (2015) 29134–29147.

[46] M.S. Minns, G. Teicher, C.B. Rich, V. Trinkaus-Randall, Purinoreceptor P2X7 regulation of Ca(2+) mobilization and cytoskeletal rearrangement is required for corneal reepithelialization after injury, Am. J. Pathol. 186 (2) (2016) 285–296.

[47] S.C. Chew, S.A. Rice, S. Kjelleberg, L. Yang, In situ mapping of the mechanical properties of biofilms by particle-tracking microrheology, J. Vis. Exp. 106 (2015) e53093.

[48] K.A. Mosiewicz, L. Kolb, A.J. van der Vlies, M.P. Lutolf, Microscale patterning of hydrogel stiffness through light-triggered uncaging of thiols, Biomater. Sci. 2 (11) (2014) 1640–1651.

[49] A. Pauli, M.L. Norris, E. Valen, G.L. Chew, J.A. Gagnon, S. Zimmerman, A. Mitchell, J. Ma, J. Dubrulle, D. Reyon, S.Q. Tsai, J.K. Joung, A. Saghatelian, A.F. Schier, Toddler: an embryonic signal that promotes cell movement via Apelin receptors, Science 343 (6172) (2014) 1248636.

[50] K. Campbell, J. Casanova, A role for E-cadherin in ensuring cohesive migration of a heterogeneous population of non-epithelial cells, Nat. Commun. 6 (2015) 7998.

[51] B. Spiesschaert, B. Goldenbogen, S. Taferner, M. Schade, M. Mahmoud, E. Klipp, N. Osterrieder, W. Azab, Role of gB and pUS3 in equine herpesvirus 1 transfer between peripheral blood mononuclear cells and endothelial cells: a dynamic in vitro model, J. Virol. 89 (23) (2015) 11899–11908.

[52] P. Schattling, B. Thingholm, B. Städler, Enhanced diffusion of glucose-fueled Janus particles, Chem. Mater. 27 (21) (2015) 7412–7418.

[53] A.H. Chen, A. Robinson-Mosher, D.F. Savage, P.A. Silver, J.K. Polka, The bacterial carbon-fixing organelle is formed by shell envelopment of preassembled cargo, PLoS ONE 8 (9) (2013) e76127.

[54] R. Müller, O. Stranik, F. Schlenk, S. Werner, D. Malsch, D. Fischer, W. Fritzsche, Optical detection of nanoparticle agglomeration in a living system under the influence of a magnetic field, J. Magn. Magn. Mater. 380 (2015) 61–65.

[55] K.G. Bondoc, J. Heuschele, J. Gillard, W. Vyverman, G. Pohnert, Selective silicate-directed motility in diatoms, Nat. Commun. 7 (2016) 10540.

[56] C. Noble, N. Smulders, N.H. Green, R. Lewis, M.J. Carré, S.E. Franklin, S. MacNeil, Z.A. Taylor, Creating a model of diseased artery damage and failure from healthy porcine aorta, J. Mech. Behav. Biomed. Mater. 60 (2016) 378–393.

[57] M. Linkert, C.T. Rueden, C. Allan, J.M. Burel, W. Moore, A. Patterson, B. Loranger, J. Moore, C. Neves, D. Macdonald, A. Tarkowska, C. Sticco, E. Hill, M. Rossner, K.W. Eliceiri, J.R. Swedlow, Metadata matters: access to image data in the real world, J. Cell Biol. 189 (5) (2010) 777–782.

[58] T. Pietzsch, S. Preibisch, P. Tomancak, S. Saalfeld, ImgLib2 – generic image processing in Java, Bioinformatics 28 (22) (2012) 3009–3011.

[59] C. Dietz, M.R. Berthold, KNIME for open-source bioimage analysis: a tutorial, Adv. Anat. Embryol. Cell Biol. 219 (2016) 179–197.

[60] N. Scherf, J. Huisken, The smart and gentle microscope, Nat. Biotechnol. 33 (8) (2015) 815–818.